Strouhal–Reynolds number relationship for flow past a circular cylinder

Hongyi Jiang[1] and Liang Cheng[1,2,†]

[1]School of Civil, Environmental and Mining Engineering, The University of Western Australia, 35 Stirling Highway, Crawley, WA 6009, Australia

[2]DUT-UWA Joint Research Centre, State Key Laboratory of Coastal and Offshore Engineering, Dalian University of Technology, Dalian, 116024, China

The Strouhal–Reynolds number (St–Re) relationship for flow past a circular cylinder in the low Re range of $Re \leqslant 1000$ is investigated through two- (2D) and three-dimensional (3D) direct numerical simulations (DNS). An improved method is proposed for the determination of the separating velocity and the wake width to allow for a better estimation of the wake Strouhal number St^*. For Re in the extended laminar regime calculated by 2D DNS, the St^* values are found to be more uniform than the original St for the 2D flow. It is also found that the St^* values for the 2D and 3D flows agree well in the laminar regime of Re up to approximately 270. In addition, uniform St^* values are also obtained for different mode A and mode B flow structures triggered artificially by using different cylinder span lengths in DNS. It is demonstrated that the drop in St (with respect to its 2D counterpart) with the development of different 3D wake structures is due to the decrease in the separating velocity and the increase in the wake width for a 3D flow, rather than the existence of a particular wake structure such as pure mode A or vortex dislocation. However, as the wake flow becomes increasingly turbulent with further increase in Re, the St^* value for the 3D flow increases gradually and deviates from its 2D counterpart, since for turbulent 3D flows the vortex shedding frequency scales on a length smaller than the wake width.

Key words: vortex shedding, vortex streets, wakes

1. Introduction

Steady incoming flow past a long smooth circular cylinder at low Reynolds numbers is one of the most classical fluid mechanics problems. In this case, the flow is governed by the Reynolds number Re ($= UD/\nu$) only, where U is the incoming flow velocity, D is the cylinder diameter and ν is the kinematic viscosity of the fluid. It is well known that for flow past a circular cylinder vortex shedding emerges at $Re = 47$ (e.g. Henderson 1997). The vortex shedding frequency f is commonly presented in a dimensionless form, namely the Strouhal number St ($= f D/U$).

† Email address for correspondence: liang.cheng@uwa.edu.au

The variation of St with Re has been studied extensively, owing to its fundamental as well as practical significance. For example, Norberg (1994) and Fey, König & Eckelmann (1998) both reported the St–Re relationship for Re from the onset of vortex shedding ($Re = 47$) to the point just before boundary layer transition ($Re \sim 2 \times 10^5$). Fey *et al.* (1998) also categorized the St–Re curve into different regimes based on different flow instabilities, such as the secondary wake instability at $Re \sim 180$ and the shear layer instability at $Re \sim 1300$. In addition, Schewe (1983) reported the St–Re relationship for Re from 2×10^4 to 7×10^6, covering the range of boundary layer transition to turbulence.

A number of empirical and semi-empirical formulae for the St–Re relationship over certain ranges of Re were proposed, for example:

(1) $St = A + B/Re$ by Roshko (1954) and Ponta & Aref (2004),
(2) $St = A + B/Re^{1/2}$ by Fey *et al.* (1998), Williamson & Brown (1998) and Ponta (2006), and
(3) $St = 1/(A + B/Re)$ by Roushan & Wu (2005),

where A and B are curve-fitting coefficients. Although some semi-empirical formulae were established by taking into account physical properties related to vortex shedding, such as the variation of the shear layer thickness with $Re^{-1/2}$ (Williamson & Brown 1998), the transport of vorticity (Ponta & Aref 2004), or the vortex street structure (Roushan & Wu 2005), the formulae were still derived ultimately through curve fitting of the actual St–Re relationship.

In the low Re range, Williamson (1996*a*) studied the St–Re relationship in the wake transition regime, and found two discontinuities in the St–Re curve:

(1) a sudden drop of St at the onset of the secondary wake instability of $Re \sim 180$, where the fully developed wake flow structure becomes mode A with large-scale vortex dislocations;
(2) a twin-peaked regime of $Re = 230$–260 where a gradual wake transition from mode A with dislocations to mode B takes place.

Williamson (1996*a*) suggested that the sudden drop of St at $Re \sim 180$ is due to the occurrence of vortex dislocations. In contrast, Henderson (1997) suggested that it is due to the mode A instability only, irrespective of the dislocations. Henderson's (1997) argument was supported by the three-dimensional (3D) direct numerical simulation (DNS) of a case at $Re = 195$ with a restricted spanwise domain length of $3.96D$. By restricting the spanwise domain length to approximately the most unstable wavelength of mode A, the fully developed wake structure is represented by one pair of ordered mode A structures, while vortex dislocation is suppressed. Nevertheless, as the 3D wake structure develops, the Strouhal number drops from its counterpart calculated by two-dimensional (2D) DNS. However, the fundamental cause for the variation of St with the development of different 3D wake structures was not revealed.

Roshko (1955) suggested that the vortex shedding frequency in the wake of a bluff body would scale better on the velocity at separation (U_s) and the wake width (D'), rather than simply on U and D. The Strouhal number based on such a definition was called the wake Strouhal number St^* ($= f D'/U_s$) in Roshko (1955). Based on experimental measurements on three bluff-body shapes, including a flat plate, a 90° wedge and a circular cylinder, Roshko (1955) obtained a relatively universal St^* of approximately 0.16 (± 0.01) for the three bodies for the wake Reynolds number Re^* ($= U_s D'/\nu$) in the range of approximately 1×10^4 to 4.4×10^4. However, relatively large and irregular discrepancies of St^* ranged between 0.16 and 0.20 were observed for Re^* below approximately 1×10^4.

By studying the experimental St^*–Re data for a circular cylinder, Williamson & Brown (1998) found a relatively universal St^* of approximately 0.176 (with variations between 0.164 and 0.186) for Re in the range of 55 to 1.4×10^5. Compared with the results reported in Roshko (1955), the more uniform St^* values in the low Re range in Williamson & Brown (1998) may be attributed to an improvement in the quality of the experimental data, for example through elimination of the 'end effect' of the cylinder (Williamson 1996*a*).

In light of the previous works, the present study aims at examining the St^*–Re relationship in the low Re range of $Re \leqslant 1000$ by using both 2D and 3D DNS. For the rest of the paper, subscripts '2D' and '3D' are used to distinguish the Strouhal numbers calculated with 2D and 3D DNS, respectively. An advantage of using DNS is that high-resolution flow properties, such as U_s and D', are available to allow for a better estimation and a thorough analysis of the 2D and 3D St^*–Re relationships. The physical mechanism for the variation of St with the development of different 3D wake structures is also investigated.

2. Numerical model

2.1. *Numerical method*

The present DNS are carried out with OpenFOAM (www.openfoam.org) to solve the continuity and incompressible Navier–Stokes equations:

$$\frac{\partial u_i}{\partial x_i} = 0, \tag{2.1}$$

$$\frac{\partial u_i}{\partial t} + u_j \frac{\partial u_i}{\partial x_j} = -\frac{1}{\rho} \frac{\partial p}{\partial x_i} + \nu \frac{\partial^2 u_i}{\partial x_j \partial x_j}, \tag{2.2}$$

where $(x_1, x_2, x_3) = (x, y, z)$ are Cartesian coordinates, u_i is the velocity component in the direction x_i, t is time, ρ is fluid density and p is pressure. The same numerical approach as used in Jiang *et al.* (2016, 2017*a,b*) is adopted here. Specifically, the finite-volume method (FVM) and the pressure-implicit with splitting of operators (PISO) algorithm (Issa 1986) are used to solve the equations.

2.2. *Computational domain and mesh*

In the present study, DNS are carried out for Re up to 1000. For $Re \leqslant 300$, the standard 2D and 3D meshes used in Jiang *et al.* (2016) are adopted. For $300 < Re \leqslant 1000$, a refined mesh over that used in Jiang *et al.* (2016) is used. Some key parameters for the standard and refined meshes are listed in table 1. Figure 1 shows a schematic model and a close-up view of the refined mesh. A relatively high mesh resolution is used in the near wake by specifying a streamwise mesh size varying linearly from $0.0375D$ at $x/D = 2$ to $0.1D$ at $x/D = 10$.

A mesh convergence check of the refined 2D and 3D meshes is reported in appendix A. In particular, a reduction in the spanwise domain length from $12D$ to $6D$ is justified, given that the relatively large-scale mode A structure (with a spanwise wavelength of $\sim 4D$) disappears at $Re \sim 270$ and the small-scale mode B structure (with a spanwise wavelength of $< 1D$) becomes the only wake flow mode for $Re > 270$. In addition, the spanwise cell length is reduced from $0.1D$ to $0.05D$, since the mode B structure becomes finer with further increase in Re.
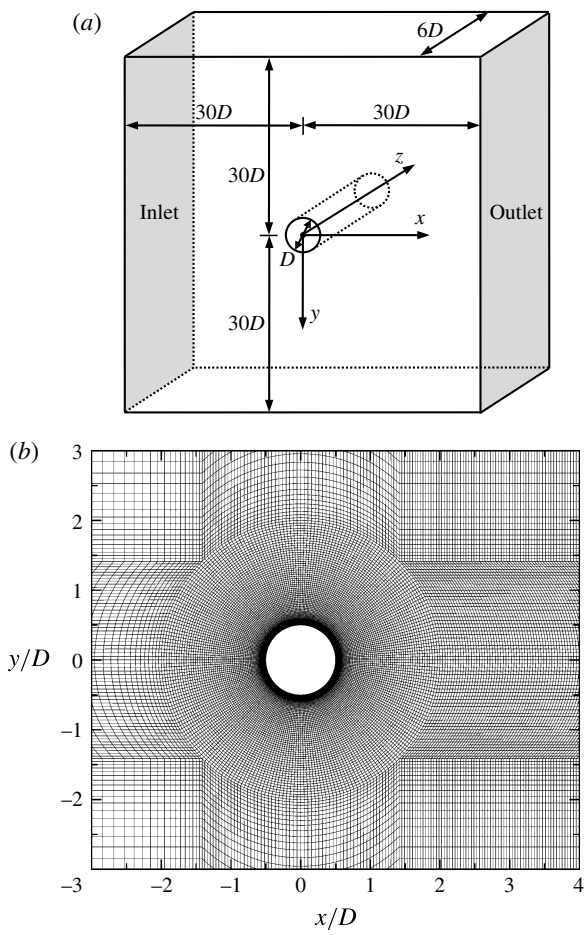
FIGURE 1. The refined mesh used for $300 < Re \leqslant 1000$: (*a*) schematic model of the computational domain, and (*b*) close-up view of the mesh near the cylinder.

Parameter	Standard mesh (for $Re \leqslant 300$)	Refined mesh (for $300 < Re \leqslant 1000$)
Distance from the cylinder centre to the inlet	$20D$	$30D$
Distance from the cylinder centre to the cross-flow boundaries	$20D$	$30D$
Distance from the cylinder centre to the outlet	$30D$	$30D$
Number of nodes around the cylinder perimeter	132	240
Height of the first layer of mesh next to the cylinder	$1 \times 10^{-3}D$	$2.315 \times 10^{-4}D$
Cell expansion ratio in the domain	$\leqslant 1.1$	$\leqslant 1.1$
Spanwise domain length for the 3D mesh	$12D$	$6D$
Spanwise cell length for the 3D mesh	$0.1D$	$0.05D$

TABLE 1. Parameters for the standard and refined meshes used in this study.

3. Determination of St_{2D}^*

3.1. *Previous method*

The wake Strouhal number St^*, as proposed by Roshko (1955), is calculated in the present study by

$$St^* = f_L D'/U_s = St \frac{U}{U_s} \frac{D'}{D}, \tag{3.1}$$

where f_L is the frequency of the fluctuating lift force. It was shown in Roshko (1955) and Williamson & Brown (1998) that St^* would be nearly constant over a wide range of Re. In both studies, U_s was calculated by

$$\frac{U_s}{U} = \sqrt{1 - C_{pb}}, \tag{3.2}$$

where C_{pb} is the base pressure coefficient defined in (A 5), which is a negative value. The wake width D' calculated in Williamson & Brown (1998) was defined as

$$\frac{D'}{D} = 1 + \frac{2\delta}{D}, \tag{3.3}$$

where δ is the separated shear layer thickness evaluated based on the time-averaged streamwise velocity profile sampled at the streamwise location of $x/D = 1$ (refer to Williamson & Brown (1998) for details).

As shown in figure 2, by adopting the method of Williamson & Brown (1998), the St_{2D}^* values for Re in the extended laminar regime up to $Re = 1000$ are indeed more uniform than the original St_{2D} values. However, based on the C_{pb} values calculated in the present DNS, it is found that (3.2) overpredicts U_s for Re larger than approximately 200, as the predicted U_s becomes increasingly larger than the maximum velocity of the whole flow field (figure 3a). In addition, the wake width calculated by (3.3) (figure 3b) is based on the streamwise velocity profile measured at a fixed streamwise location of $x/D = 1$, whereas for 2D flows the streamwise length of the recirculation region reduces monotonically with increasing Re and the vortices may roll up well before $x/D = 1$ (see figure 7a for an example at $Re = 1000$), such that the wake width measured at $x/D = 1$ may not represent the actual wake width that initiates the vortex rolling up and shedding. Nevertheless, for Re larger than approximately 200, the overpredictions of both U_s and D' by using (3.2) and (3.3) do not necessarily lead to an inaccurate prediction of St_{2D}^*, since the overpredictions of U_s and D' are incidentally at a similar level and thus cancel out in (3.1).

3.2. *An improved method*

In the present study, an improved method is proposed for the determination of U_s and D'. It is important to note that the U_s value should be considered as a velocity representative of the regional flow field near the separation, rather than the velocity at a particular point. This is because the velocity profile still develops as the flow travels from the separation point to the point where vortices start to roll up, and the vortex shedding frequency is affected by the velocity at the latter point. In this study, U_s is chosen as the peak value ($u_{x,max}$) along the time-averaged streamwise velocity (u_x) profile at $x/D = 0$, as denoted by a solid dot in figure 4(a). The reason for the choice of U_s is illustrated in figure 4(b) with the u_x profile for $Re = 100$ as an example. In
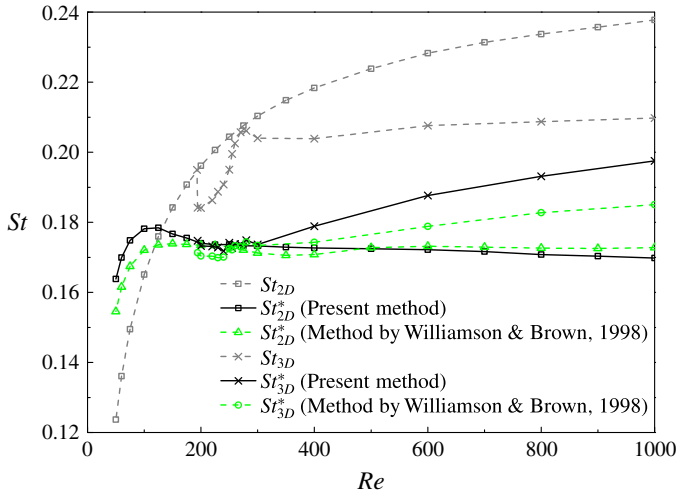
FIGURE 2. (Colour online) The 2D and 3D *St–Re* relationships for flow past a circular cylinder.

figure 4(b), the shear layer vorticity thickness δ_ω is calculated as (Monkewitz 1988):

$$\delta_\omega = \frac{u_{x,max}}{|\mathrm{d}u_x/\mathrm{d}y|_{max}}. \tag{3.4}$$

The separated shear layer thickness δ is calculated as $\delta = \delta_\omega/2$ (Williamson & Brown 1998), and the streamwise velocity at point B, namely the midpoint of line AC, is $u_{x,max}/2$. As shown in figure 4(b), line AB serves as a good approximation of the u_x profile along the separating shear layer, and therefore $u_{x,max}/4$ is considered to be a good approximation of the mean streamwise velocity within the shear layer. In the present study, U_s is chosen as $u_{x,max}$ rather than as $u_{x,max}/2$ or $u_{x,max}/4$ so as to facilitate comparison with the results of Williamson & Brown (1998). The U_s–Re relationship based on the present method is plotted in figure 3(a).

On the other hand, the D' value in the present study is determined directly based on the spanwise vorticity contours of the time-averaged flow field. The spanwise vorticity ω_z is defined in a non-dimensional form as

$$\omega_z = \left(\frac{\partial u_y}{\partial x} - \frac{\partial u_x}{\partial y} \right) \frac{D}{U}. \tag{3.5}$$

As illustrated in figure 5, D' is chosen as the largest vertical distance between the positive and negative ω_z peaks. The D'–Re relationship based on the present method is plotted in figure 3(b).

It is also worth noting that, if the time-averaged streamwise velocity profile sampled at the streamwise location of the largest vertical distance between the positive and negative ω_z peaks, rather than fixed at $x/D = 1$ as suggested by Williamson & Brown (1998), is used in (3.3) for the determination of D', the D' value would be within 3 % of that determined based on the spanwise vorticity field (figure 3b). This suggests that the major improvement of the present method over (3.3) is in the choice of the streamwise location for the determination of D'. This streamwise location should be upstream of the location where vortices start to roll up. In addition, the present method
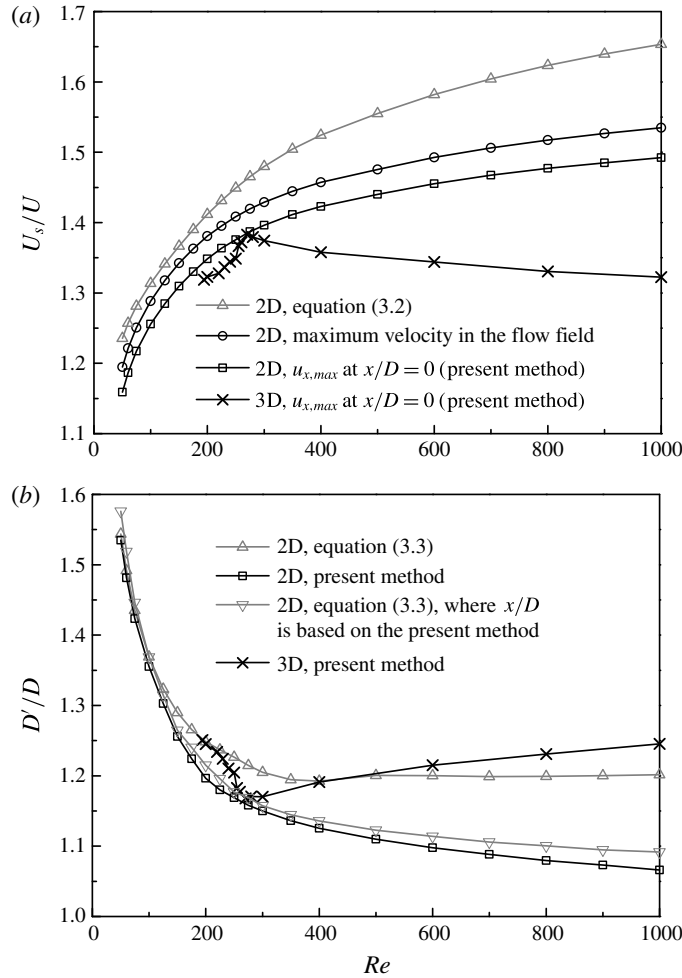
FIGURE 3. The (*a*) U_s–Re and (*b*) D'–Re relationships, evaluated based on different methods.

uses the spanwise vorticity field instead of the streamwise velocity profile to evaluate D'. This is because the spanwise vorticity field (e.g. figure 5) reveals directly the vertical extent for the vortices to roll up to trigger vortex shedding, while in (3.3) the separated shear layer thickness is evaluated indirectly based on a linear approximation of the streamwise velocity profile.

The St_{2D}^*–Re relationship based on the present U_s and D' results is also plotted in figure 2, where the St_{2D}^* values are found to be more uniform than the St_{2D} values. However, it is worth noting that the St_{2D}^* values are still not completely uniform. This is because, although the vortex shedding frequency scales primarily on U_s and D', it may still be influenced by other secondary factors such as the redistribution of the velocity profile in the near wake. This is not explored further in this study. The rest of the paper will focus on the comparison of 2D and 3D vortex shedding frequencies.
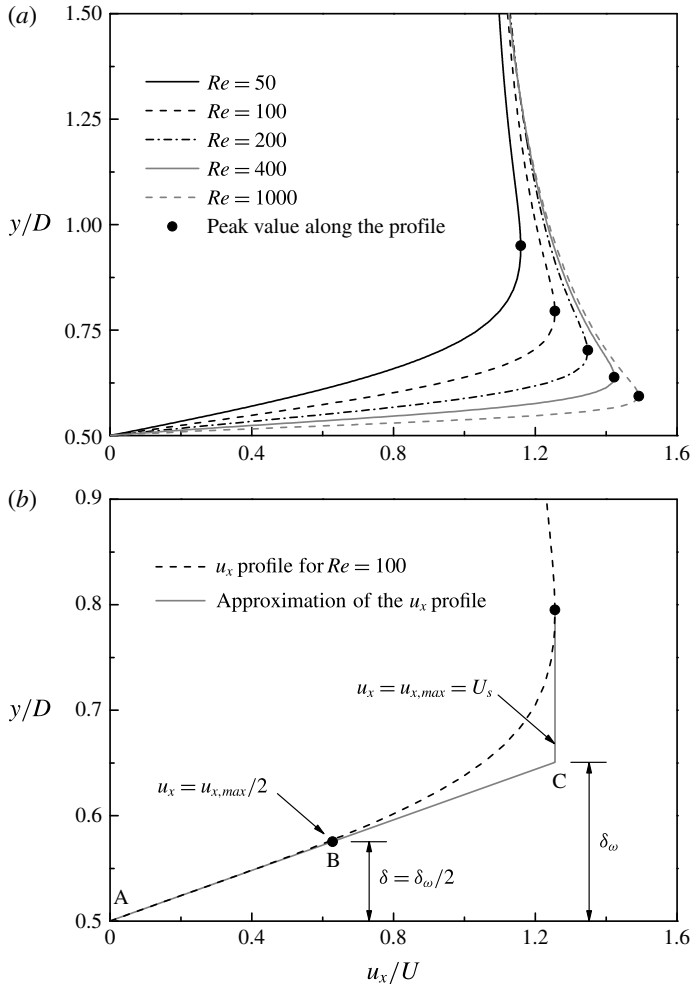
FIGURE 4. Time-averaged streamwise velocity profiles sampled at $x/D = 0$: (*a*) for various *Re* values, and (*b*) for $Re = 100$.

4. Determination of St_{3D}^*

4.1. *The St_{3D}^*–Re relationship*

The method proposed in §3.2 is extended for the study of the 3D flows. Since the 3D flow beyond the secondary wake instability may not be regular periodic with the evolution in time, at least 1000 non-dimensional time units of the fully developed flow have been used for the calculation of the time-averaged flow. By further averaging the time-averaged flow along the spanwise direction, a 2D flow field is obtained and is then used for the determination of U_s and D' (the results are also shown in figure 3).

As reported in Williamson (1996*a*), in the mode swapping regime of approximately $Re = 230$–260, two different St_{3D} values exist for each *Re*, i.e. a lower St_{3D} for mode A with dislocations and a higher St_{3D} for mode B. In the present study, however, as the time-averaged flow is considered, the original St_{3D} is calculated based on the time-averaged frequency of the fluctuating lift force, rather than through the fast
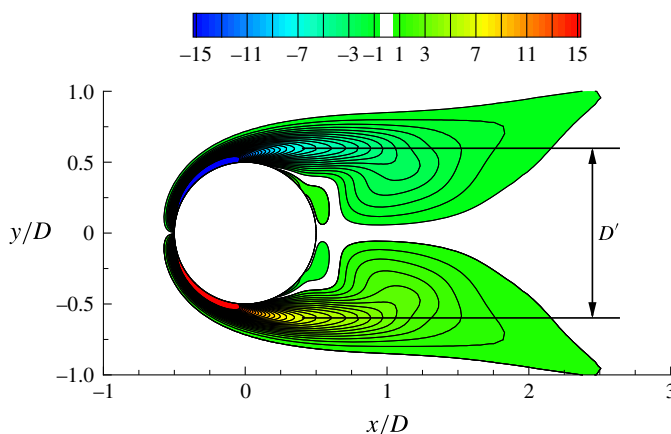
FIGURE 5. (Colour online) Determination of D' based on the spanwise vorticity contours of the time-averaged 2D flow field at $Re = 200$.

Fourier transform (FFT) analysis of the lift force time history, such that only one time-averaged St_{3D} value is obtained for each Re (figure 2).

As shown in figure 2, for the laminar regime of Re up to approximately 270, St_{3D}^* matches St_{2D}^* very well. However, as the wake flow becomes increasingly turbulent with further increase in Re, St_{3D}^* increases gradually and deviates from the corresponding St_{2D}^* value. This suggests that for turbulent flows the vortex shedding frequency no longer scales on U_s and D'.

4.2. *Physical mechanism for the deviation between St_{3D}^* and St_{2D}^**

As summarized in Williamson (1996*b*), for the range of Re from the onset of wake turbulence at $Re \sim 270$ to the onset of shear layer instability at $Re \sim 1200$, the mode B structure in the near wake becomes increasingly disordered, which results in a reduction in the 2D Reynolds stresses in the near wake, a consistent reduction in the base pressure and an increase in the formation length (L_f) as shown in figure 6. These variations are also consistent with the reduction in U_s and the increase in D' for $Re = 270$–1000 shown in figure 3.

The physical mechanism for the deviation between St_{3D}^* and St_{2D}^* is examined at $Re = 1000$. Figure 7 shows the instantaneous ω_z contours of the 2D and 3D (averaged over the span) flows at $Re = 1000$, at the time instant that the maximum u_x at $x/D = 0$ is the largest on the upper side of the cylinder and the smallest on the lower side of the cylinder, namely at the instant when u_x on the lower side of the cylinder starts to increase. At this point, a positive vortex has just been shed from the lower shear layer, and the lower shear layer is about to roll up to form a new vortex. As shown in figure 7(*a*), the shedding of the positive vortex in the 2D flow is to a great extent influenced by the rolling up of the negative vortex from the opposite side of the cylinder. For the 3D flow, however, as the recirculation region is much longer (as indicated by the wake stagnation point in figure 7), the lower separating shear layer becomes longer and thus weaker at the point of shedding (figure 7*b*). Therefore, the positive vortex in the 3D flow is shed more independently, at a point that the negative vortex from the opposite side of the cylinder is still relatively far away from the lower shear layer. In other words, the cross-flow distance for the negative vortex to roll up
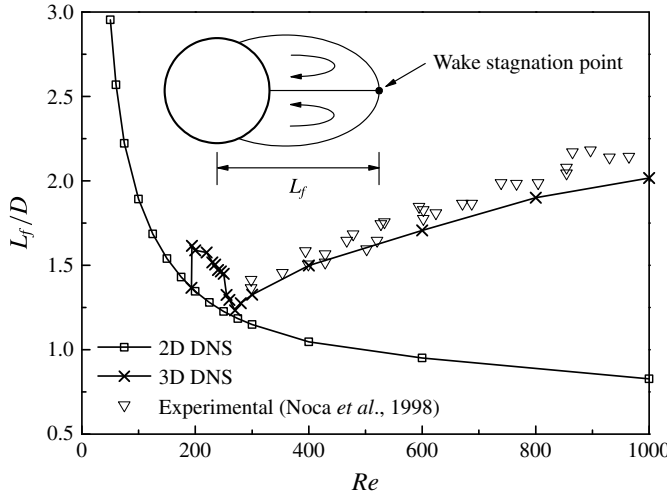
FIGURE 6. The 2D and 3D L_f–Re relationships for flow past a circular cylinder.

to trigger the shedding of the positive vortex is reduced. Consequently, the vortex shedding frequency of the 3D flow would scale on a length smaller than that for the 2D flow. When D' is used for the determination of both St^*_{2D} and St^*_{3D}, St^*_{3D} would be larger than St^*_{2D}, as is manifested in figure 2.

Generally, the deviation between St^*_{3D} and St^*_{2D} is observed at $Re > 300$ (figure 2), for which the increasing deviation between formation lengths calculated by 2D and 3D DNS (figure 6) gradually becomes a third major factor influencing the vortex shedding frequency.

5. Strouhal numbers for modes A and B

For the laminar regime, which includes mode A and the onset of mode B, an agreement of St^*_{3D} and St^*_{2D} is observed in figure 2, while the difference in the St_{3D} and St_{2D} values is attributed to the different U_s and D' values used for the 2D and 3D flows to transform St^* into the corresponding St. This suggests that the drop of St_{3D} from its St_{2D} counterpart is also due to the decrease in U_s and the increase in D' for a 3D flow (figure 3).

The decrease in U_s in a 3D flow is related to the spanwise energy amplification of the shear layers. The decrease in U_s also results in a thicker shear layer and thus an increase in D'. Therefore, similar variation trends for the degree of deviation between St_{3D} and St_{2D} and the flow three-dimensionality are observed (figure 8). The deviation between St_{3D} and St_{2D} is calculated as

$$\Delta St = (St_{2D} - St_{3D})/St_{2D} \times 100\,\%. \tag{5.1}$$

The flow three-dimensionality is represented by the statistically stationary spanwise kinetic energy E_z integrated over the near-wake region of $x/D = 0$–10, where E_z is defined as

$$E_z = \frac{1}{2} \int_V (u_z/U)^2 \, \mathrm{d}V, \tag{5.2}$$

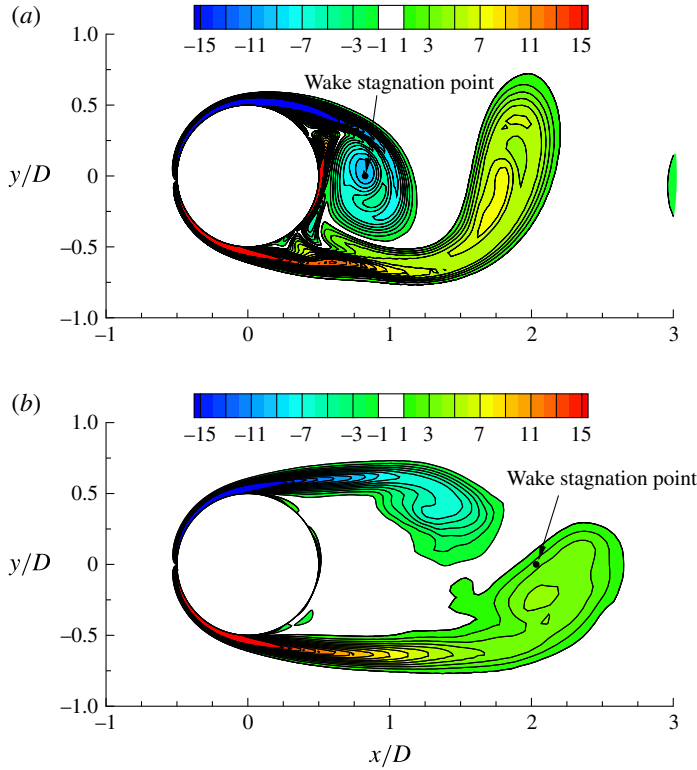where V is the volume of the flow field of interest.

FIGURE 7. (Colour online) Instantaneous ω_z contours for flow past a circular cylinder at $Re = 1000$: (*a*) the 2D flow, and (*b*) the 3D flow (averaged over the span). The wake stagnation point obtained from the time-averaged flow field is marked by a solid dot.
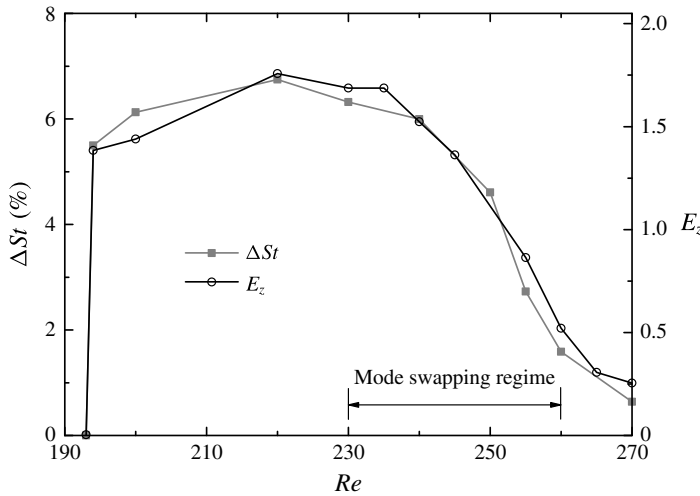

FIGURE 8. Variation trends for the degree of deviation between St_{3D} and St_{2D} (ΔSt) and the flow three-dimensionality (represented by E_z).
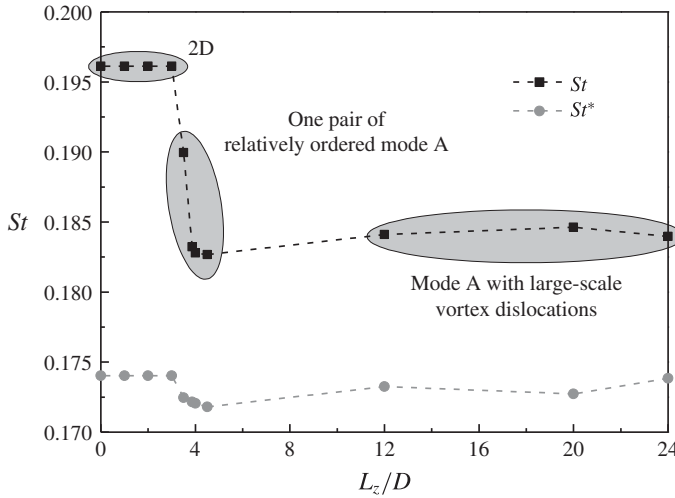
FIGURE 9. Variation of St with L_z for the mode A flow at $Re = 200$.

The Strouhal number for the mode A flow is further studied at $Re = 200$ through varying the cylinder span length L_z to obtain different mode A flow structures. The variation of St with L_z is shown in figure 9. The flow is 2D for $L_z/D \leqslant 3$ but becomes unstable to mode A instability for $L_z/D \geqslant 3.5$, which is consistent with the neutral instability curve for mode A proposed by Barkley & Henderson (1996). Figure 10 shows some typical mode A wake flow structures in the fully developed state, identified by the isosurfaces of the streamwise vorticity ω_x:

$$\omega_x = \left(\frac{\partial u_z}{\partial y} - \frac{\partial u_y}{\partial z} \right) \frac{D}{U}. \tag{5.3}$$

For $L_z/D \geqslant 12$, the fully developed flow is represented by mode A with large-scale vortex dislocations (e.g. figure 10c), which is consistent with the experimental results (e.g. Williamson 1996a). In contrast, for L_z comparable to the most unstable spanwise wavelength of mode A of $\lambda_A = 3.865D$ at $Re = 200$, the fully developed flow is represented by one pair of ordered mode A structures (e.g. figure 10a,b), while vortex dislocation is suppressed due to the confinement of a short span length (Henderson 1997).

Based on the observation of an obvious drop of St_{3D} with the development of ordered mode A structures under the restriction of $L_z = \lambda_A$ at $Re = 195$, Henderson (1997) suggested that the drop of St_{3D} is due to the existence of the pure mode A structure rather than vortex dislocation. This is consistent with the present results at $Re = 200$ shown in figures 9 and 10, where the St_{3D} value for $L_z = \lambda_A = 3.865D$ (with pure mode A) is very close to those for $L_z \geqslant 12D$ (with dislocations). However, for the pure mode A flow calculated with $L_z = 3.5D$ (figure 10a), the St_{3D} value is not in line with those for $L_z = 3.865D$ or $L_z \geqslant 12D$. This cannot be explained by Henderson's (1997) argument.

As shown in figure 9, although the vortex structures and St may be different for the cases with different L_z, the St^* values are quite uniform. This suggests that the drop of St_{3D} is largely due to the decrease in U_s and the increase in D' for a 3D
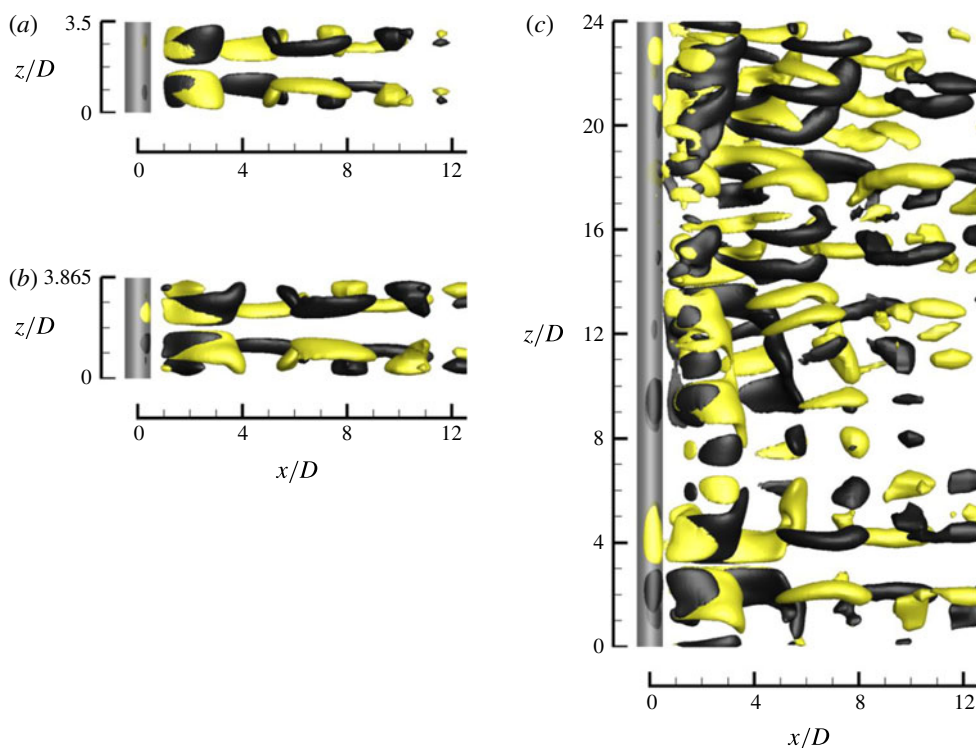
FIGURE 10. (Colour online) Mode A wake flow structures in the fully developed state at $Re = 200$: (a) with $L_z/D = 3.5$, (b) with $L_z/D = 3.865$ and (c) with $L_z/D = 24$. The wake structures are captured by the isosurfaces of $\omega_x = \pm 0.5$. Dark grey and light yellow denote positive and negative values, respectively. The flow is from the left to the right past the cylinder on the left.

flow, rather than the existence of a particular wake structure such as pure mode A or vortex dislocation.

The same mechanism also holds for the Strouhal number for the mode B flow. The mode B flow is analysed at $Re = 300$ rather than at the onset of wake turbulence of $Re = 270$ because at $Re = 300$ an obvious drop of St_{3D} is observed while the deviation between St_{3D}^* and St_{2D}^* is still negligibly small (figure 2). Figure 11 shows the variation of St with L_z for the mode B flow at $Re = 300$. The wake flow is represented by one or two pairs of ordered mode B structures at small L_z (e.g. figure 12a–c) but becomes disordered at large L_z (e.g. figure 12d). Similar to the results of the mode A flow shown in figure 9, the St^* values shown in figure 11 for the mode B flow are also quite uniform, regardless of the different vortex structures and St values under different L_z.

6. Conclusions

This paper examines both the 2D and 3D St–Re relationships for flow past a circular cylinder in the low Re range of $Re \leqslant 1000$ through DNS. An improved method is proposed for the determination of the separating velocity U_s and the wake width D' to allow for a better estimation of the wake Strouhal number St^*.
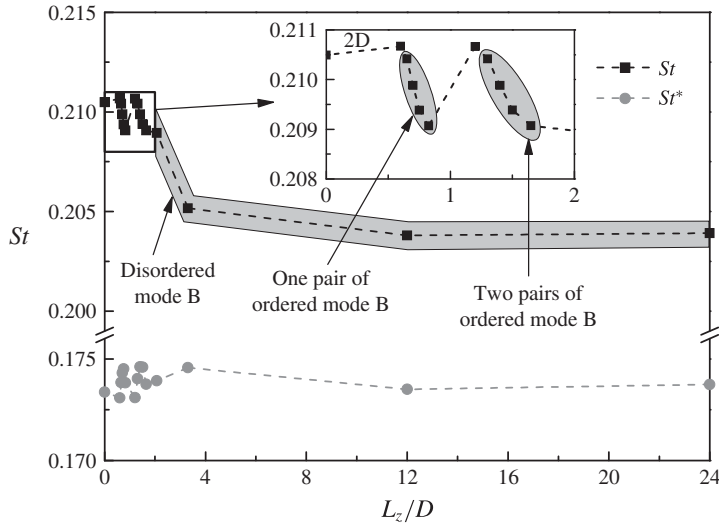
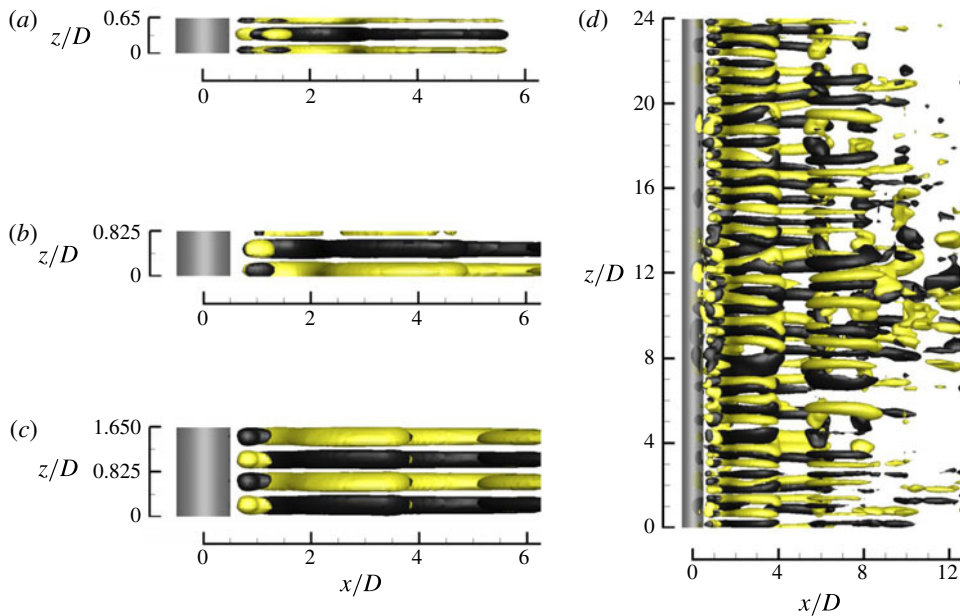FIGURE 11. Variation of St with L_z for the mode B flow at $Re = 300$.

FIGURE 12. (Colour online) Mode B wake flow structures in the fully developed state at $Re = 300$ with (a) $L_z/D = 0.65$, (b) $L_z/D = 0.825$, (c) $L_z/D = 1.65$ and (d) $L_z/D = 24$. The wake structures are captured by the isosurfaces of $\omega_x = \pm 0.5$. Dark grey and light yellow denote positive and negative values, respectively. The flow is from the left to the right past the cylinder on the left.

Based on 2D DNS, it is found that the St_{2D}^* values for Re in the extended laminar regime are more uniform than the original St_{2D} values, since the 2D vortex shedding frequency scales primarily on U_s and D'. Based on 3D DNS, it is found that St_{3D}^*

matches St^*_{2D} well for the laminar regime of *Re* up to approximately 270. However, as the wake flow becomes increasingly turbulent with further increase in *Re*, St^*_{3D} increases gradually and deviates from the corresponding St^*_{2D} value. This is because the increase in the streamwise length of the recirculation region results in a weaker separating shear layer at the point of vortex shedding, such that vortex shedding is less influenced by the rolling up of the vortex from the opposite side of the cylinder. Owing to a reduced cross-flow distance for the vortex from the opposite side of the cylinder to roll up to trigger vortex shedding, the vortex shedding frequency scales on a length that is smaller than D'.

For both the mode A and mode B flows in the laminar regime, in addition to the agreement of St^*_{2D} and St^*_{3D} by using a relatively large cylinder span length of $L_z = 12D$, uniform St^* values are also obtained by using different L_z, regardless of the different wake structures and St due to the restriction of L_z. This suggests that the drop of St_{3D} from St_{2D} with the development of different 3D wake structures is due to the decrease in the separating velocity and the increase in the wake width for a 3D flow, rather than the existence of a particular wake structure such as pure mode A or vortex dislocation.

Acknowledgements

Appendix A. Mesh convergence

The time step Δt adopted for each case is based on the criterion that the maximum Courant number (Co_{max}) in the computational domain is kept below 0.4. The Courant number for a cell is defined as

$$Co = |u|\Delta t/\Delta l, \tag{A 1}$$

where $|u|$ is the magnitude of the velocity through a cell, and Δl is the cell size in the direction of the velocity.

A mesh dependence study on the refined 2D mesh is carried out at $Re = 1000$ (the largest *Re* adopted in this study) with the following three variations.

(1) Increase in the domain size. The distance from the cylinder centre to each side of the domain is increased from $30D$ to $60D$.
(2) Increase in the mesh resolution. The number of cells in both *x* and *y* directions is doubled. In particular, the number of nodes around the cylinder surface is doubled from 240 to 480, and the height of the first layer of mesh next to the cylinder surface is halved from $2.315 \times 10^{-4}D$ to $1.174 \times 10^{-4}D$.
(3) Decrease in the time step size. The time step size is reduced to 20 % of that before through keeping Co_{max} below 0.08.

The mesh convergence is checked by examining the variations in the hydrodynamic forces on the cylinder. The hydrodynamic forces, including the drag and lift force coefficients (C_D and C_L), the Strouhal number (St) and the base pressure coefficient (C_{pb}) are defined as follows:

$$C_D = F_D/(\rho DU^2 L_z/2), \tag{A 2}$$

Case description	St	$\overline{C_D}$	C_L'	$-C_{pb}$
Refined 2D mesh (reference case)	0.2377	1.513	1.031	1.734
Increase in the domain size	0.2374	1.505	1.029	1.718
Increase in the mesh resolution	0.2390	1.521	1.042	1.752
Decrease in the time step size	0.2380	1.514	1.036	1.735
Henderson (1997), DNS	0.237	1.505	—	—

TABLE 2. Results of the 2D mesh dependence study at $Re = 1000$.

No.	Case description	L_z/D	$\Delta z/D$	St	$\overline{C_D}$	C_L'	$-C_{pb}$
1	Refined 3D mesh (reference case)	6	0.05	0.2105	1.0138	0.1191	0.8373
2	Increase in L_z	12	0.05	0.2098	1.0104	0.1063	0.8320
3	Decrease in Δz	6	0.03	0.2106	1.0002	0.0998	0.8148
4	Increase in Δz	6	0.0706	0.2111	1.0420	0.1597	0.8759
5	Further increase in Δz	6	0.1	0.2125	1.0467	0.1624	0.8836
	Papaioannou *et al.* (2006), DNS	3π	0.147	0.216	1.030	—	0.815
	Tong, Cheng & Zhao (2015), DNS	10	0.1	0.215	1.08	0.20	0.89
	Williamson & Brown (1998), expt.	—	—	0.212	—	—	—
	Norberg (1994), expt.	—	—	0.210	—	—	0.810

TABLE 3. Results of the 3D mesh dependence study at $Re = 1000$.

$$C_L = F_L/(\rho DU^2 L_z/2), \qquad (A\,3)$$

$$St = f_L D/U, \qquad (A\,4)$$

$$C_{pb} = (p_b - p_\infty)/(\rho U^2/2), \qquad (A\,5)$$

where F_D and F_L are the integrated drag force and lift force on the cylinder, respectively, L_z is the spanwise domain length, f_L is the frequency of the fluctuating lift force, p_b is the time-averaged pressure at the rear stagnation point of the cylinder and p_∞ is the reference pressure at the inlet of the domain. The time-averaged drag and lift coefficients are denoted as $\overline{C_D}$ and $\overline{C_L}$, respectively. The root-mean-square lift coefficient C_L' is defined as

$$C_L' = \sqrt{\frac{1}{N} \sum_{i=1}^{N} (C_{L,i} - \overline{C_L})^2}, \qquad (A\,6)$$

where N is the number of values in the time history of C_L.

The results of the 2D mesh dependence study are listed in table 2. With respect to the reference case with the refined 2D mesh, the largest variations in the hydrodynamic forces for the three variation cases are approximately 1 %. In addition, the St and $\overline{C_D}$ values calculated with the refined 2D mesh are very close to those calculated by Henderson (1997). The above results suggest that the refined 2D mesh is adequate for the present study with $Re \leqslant 1000$.

The 3D mesh dependence study focuses on the mesh resolution and domain size in the spanwise direction. The reference case for the 3D mesh dependence study is the refined 3D mesh, which is formed by replicating the refined 2D mesh along the z-axis with $L_z/D = 6$ and a uniform spanwise cell length of $\Delta z/D = 0.05$. Table 3 lists the

numerical cases and results for the 3D mesh dependence study at $Re = 1000$. At least 800 non-dimensional time units (defined as $t^* = Ut/D$) of the fully developed flow are used to calculate the statistical stationary hydrodynamic forces on the cylinder. The St value for the 3D flow is determined using the peak frequency derived from the FFT of the time history of the lift coefficient.

With respect to the reference case (case 1) in table 3, case 2 is designed to examine the adequacy of L_z. It is found that an L_z of 6D is sufficient for the simulation at $Re = 1000$, since an increase in L_z to 12D results in very close numerical results. Note that C'_L may decrease to a small extent, since with increasing L_z the integrated lift coefficient is more likely to be cancelled out by the phase differences along the span (Henderson 1997). On the other hand, cases 3–5 are designed to examine the influence of Δz. Relatively small variations of the hydrodynamic forces are observed when Δz decreases from 0.1D to 0.0706D (case 5 to case 4) and from 0.05D to 0.03D (case 1 to case 3), whereas more dramatic variations of the hydrodynamic forces are observed when Δz decreases from 0.0706D to 0.05D (case 4 to case 1). As a compromise between numerical accuracy and computational cost, the reference case with $\Delta z/D = 0.05$ (case 1 in table 3) is adopted for the 3D simulations in this study for $Re = 400$–1000. It is also seen in table 3 that the hydrodynamic forces predicted with the reference case are in close agreement with the experimental results reported in Norberg (1994) and Williamson & Brown (1998).

While it was demonstrated in Jiang *et al.* (2016) that the standard 3D mesh with $\Delta z/D = 0.1$ is adequate for $Re \leqslant 300$, the cases listed in table 3 suggest that at least $\Delta z/D = 0.05$ is required for $Re = 1000$. As shown in figure 13, this is because the streamwise vortices of mode B become finer with increasing Re, and therefore a finer mesh resolution in the spanwise direction, namely a smaller Δz, is required to resolve the finer mode B structures. The decrease of the $\overline{C_D}$, C'_L and $-C_{pb}$ values as $\Delta z/D$ decreases from 0.0706D to 0.05D (table 3) is also due to a refined resolution of the mode B structures and consequently an increase in the flow three-dimensionality. Consistently, for the DNS results reported in Tong *et al.* (2015) by using a very similar numerical formulation to that adopted in the present study, the use of $\Delta z/D = 0.1$ for $Re = 1000$ resulted in overpredicted $\overline{C_D}$, C'_L and $-C_{pb}$ values (table 3).

By using the refined 3D mesh as a replacement for the standard 3D mesh for $Re > 300$, the number of spanwise mesh layers per unit span length is doubled. This was the incentive for the use of a halved L_z of 6D for the refined 3D mesh so as to keep the computational cost at an affordable level. For $Re < 270$, due to the existence of the relatively large-scale mode A structure (with a spanwise wavelength of $\sim 4D$) and the associated vortex dislocation, $L_z > 10D$ is necessary for the prediction of converged numerical results (Jiang, Cheng & An 2017*c*). With further increase in Re, the small-scale mode B structure (with a spanwise wavelength of $<1D$) becomes the only wake flow mode, which offers theoretical support for the use of a reduced L_z. This is demonstrated with the 3D mesh dependence study at $Re = 400$. As shown in table 4, similar numerical results are obtained when L_z/D reduces from 12 to 6 (case 3 to case 2 in table 4). In addition, it is found that the numerical results at $Re = 400$ (case 2 to case 1 in table 4) are less sensitive to the decrease in $\Delta z/D$ from 0.1 to 0.05 than those at $Re = 1000$ (case 5 to case 1 in table 3), which suggests that $\Delta z/D = 0.05$ should also be sufficient for $Re = 400$. Hence, in the present study, the refined 3D mesh with $L_z/D = 6$ and $\Delta z/D = 0.05$ is adopted for the range of $Re = 400$–1000 for consistency.
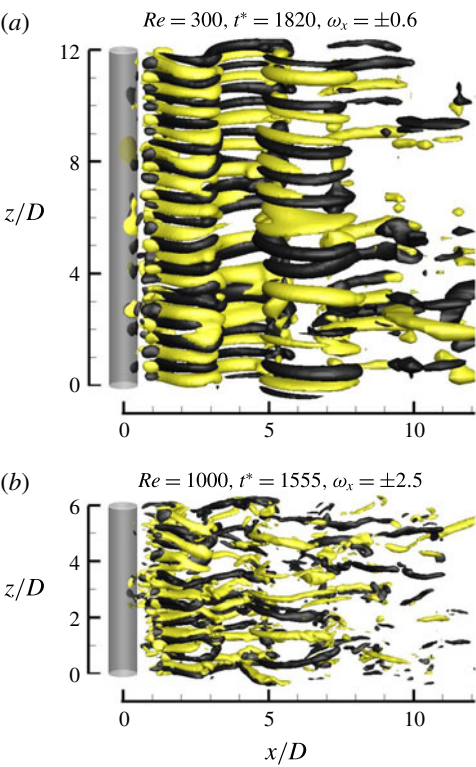
FIGURE 13. (Colour online) Isosurfaces of ω_x for the fully developed mode B structures at (*a*) $Re = 300$ with the standard 3D mesh ($L_z/D = 12$ and $\Delta z/D = 0.1$), and (*b*) $Re = 1000$ with the refined 3D mesh ($L_z/D = 6$ and $\Delta z/D = 0.05$). Dark grey and light yellow denote positive and negative values, respectively. The flow is from the left to the right past the cylinder on the left.

No.	Case description	L_z/D	$\Delta z/D$	St	$\overline{C_D}$	C'_L	$-C_{pb}$
1	Refined 3D mesh	6	0.05	0.2039	1.1960	0.3355	0.9674
2	Increase in Δz	6	0.1	0.2049	1.2187	0.3793	1.0020
3	Increase in both L_z and Δz	12	0.1	0.2045	1.2109	0.3594	0.9898

TABLE 4. Results of the 3D mesh dependence study at $Re = 400$.

REFERENCES

BARKLEY, D. & HENDERSON, R. D. 1996 Three-dimensional Floquet stability analysis of the wake of a circular cylinder. *J. Fluid Mech.* **322**, 215–241.

FEY, U., KÖNIG, M. & ECKELMANN, H. 1998 A new Strouhal–Reynolds-number relationship for the circular cylinder in the range $47 < Re < 2 \times 10^5$. *Phys. Fluids* **10**, 1547–1549.

HENDERSON, R. D. 1997 Nonlinear dynamics and pattern formation in turbulent wake transition. *J. Fluid Mech.* **352**, 65–112.

ISSA, R. I. 1986 Solution of implicitly discretized fluid flow equations by operator-splitting. *J. Comput. Phys.* **62**, 40–65.

JIANG, H., CHENG, L. & AN, H. 2017c On numerical aspects of simulating flow past a circular cylinder. *Intl J. Numer. Meth. Fluids* **85**, 113–132.

JIANG, H., CHENG, L., DRAPER, S. & AN, H. 2017a Two- and three-dimensional instabilities in the wake of a circular cylinder near a moving wall. *J. Fluid Mech.* **812**, 435–462.

JIANG, H., CHENG, L., DRAPER, S. & AN, H. 2017b Three-dimensional wake transition for a circular cylinder near a moving wall. *J. Fluid Mech.* **818**, 260–287.

JIANG, H., CHENG, L., DRAPER, S., AN, H. & TONG, F. 2016 Three-dimensional direct numerical simulation of wake transitions of a circular cylinder. *J. Fluid Mech.* **801**, 353–391.

MONKEWITZ, P. A. 1988 The absolute and convective nature of instability in two-dimensional wakes at low Reynolds numbers. *Phys. Fluids* **31**, 999–1006.

NOCA, F., PARK, H. & GHARIB, M. 1998 Vortex formation length of a circular cylinder ($300 < Re < 4000$) using DPIV. *Proceedings on Bluff Body Wakes and Vortex-Induced Vibration*. ASME Fluids Engineering Division.

NORBERG, C. 1994 An experimental investigation of the flow around a circular cylinder: influence of aspect ratio. *J. Fluid Mech.* **258**, 287–316.

PAPAIOANNOU, G. V., YUE, D. K. P., TRIANTAFYLLOU, M. S. & KARNIADAKIS, G. E. 2006 Three-dimensionality effects in flow around two tandem cylinders. *J. Fluid Mech.* **558**, 387–413.

PONTA, F. L. 2006 Effect of shear-layer thickness on the Strouhal–Reynolds number relationship for bluff-body wakes. *J. Fluids Struct.* **22**, 1133–1138.

PONTA, F. L. & AREF, H. 2004 Strouhal–Reynolds number relationship for vortex streets. *Phys. Rev. Lett.* **93**, 084501.

ROSHKO, A. 1954 On the development of turbulent wakes from vortex streets. National Advisory Committee for Aeronautics Report 1191.

ROSHKO, A. 1955 On the wake and drag of bluff bodies. *J. Aeronaut. Sci.* **22**, 124–132.

ROUSHAN, P. & WU, X. L. 2005 Structure-based interpretation of the Strouhal–Reynolds number relationship. *Phys. Rev. Lett.* **94**, 054504.

SCHEWE, G. 1983 On the force fluctuations acting on a circular cylinder in crossflow from subcritical up to transcritical Reynolds numbers. *J. Fluid Mech.* **133**, 265–285.

TONG, F., CHENG, L. & ZHAO, M. 2015 Numerical simulations of steady flow past two cylinders in staggered arrangements. *J. Fluid Mech.* **765**, 114–149.

WILLIAMSON, C. H. K. 1996a Three-dimensional wake transition. *J. Fluid Mech.* **328**, 345–407.

WILLIAMSON, C. H. K. 1996b Vortex dynamics in the cylinder wake. *Annu. Rev. Fluid Mech.* **28**, 477–539.

WILLIAMSON, C. H. K. & BROWN, G. L. 1998 A series in $1/\sqrt{Re}$ to represent the Strouhal–Reynolds number relationship of the cylinder wake. *J. Fluids Struct.* **12**, 1073–1085.